High-precision ^{28}Si(p,t)^{26}Si reaction to determine ^{22}Mg(α,p)^{25}Al reaction rates

A. Matic,[*] A. M. van den Berg, M. N. Harakeh,[†] and H. J. Wörtche[‡]
Kernfysisch Versneller Instituut, University of Groningen, Zernikelaan 25, NL-9747 AA Groningen, The Netherlands

M. Beard, G. P. A. Berg, J. Görres, P. LeBlanc, S. O'Brien, and M. Wiescher
Department of Physics and the Joint Institute for Nuclear Astrophysics, University of Notre Dame, Notre Dame, Indiana 46556, USA

K. Fujita, K. Hatanaka, Y. Sakemi, Y. Shimizu,[§] Y. Tameshige,[‖] A. Tamii, and M. Yosoi
Research Center for Nuclear Physics, Osaka University, Ibaraki, Osaka 560-0047, Japan

T. Adachi, Y. Fujita, and Y. Shimbara
Department of Physics, Osaka University, Toyonaka, Osaka 560-0043, Japan

H. Fujita
School of Physics, University of the Witwatersrand, PO Wits, Johannesburg 2050, South Africa

T. Wakasa
Department of Physics, Kyushu University, Fukuoka 812-8581, Japan

J. P. Greene
Physics Division, Argonne National Laboratory, 9700 S. Cass. Avenue, Argonne, Illinois 60439, USA

R. Crowter
Department of Physics, University of Surrey, United Kingdom

H. Schatz
National Superconducting Cyclotron Laboratory, Michigan State University, East Lansing, Michigan 48824, USA
(Received 18 April 2011; revised manuscript received 7 July 2011; published 24 August 2011)

The rise time of stellar x-ray bursts is a signature of thermonuclear runaway processes in the atmosphere of neutron stars and is highly sensitive to a series of (α,p) reactions via high-lying resonances in sd-shell nuclei. Lacking data for the relevant resonance levels, the stellar reaction rates have been calculated using statistical, Hauser-Feshbach models, assuming a high-level density. This assumption may not be correct in view of the selectivity of the (α,p) reaction to natural parity states. We measured the ^{28}Si(p,t)^{26}Si reaction with a high-resolution spectrometer to identify resonance levels in ^{26}Si above the α-emission threshold at 9.164 MeV excitation energy. These resonance levels are used to calculate the stellar reaction rate of the ^{22}Mg(α,p)^{25}Al reaction and to test the validity of the statistical assumption.

DOI: 10.1103/PhysRevC.84.025801 PACS number(s): 25.40.Hs, 26.30.Ca, 26.50.+x, 27.30.+t

I. INTRODUCTION

Stellar x-ray bursts (XRB) are frequently observed phenomena interpreted as a signature for thermonuclear runaway processes in the atmosphere of accreting neutron stars [1]. The runaway process is triggered by the breakout of the hot CNO cycles and fueled by the triple-alpha process converting three alpha particles to ^{12}C. The breakout process is initiated by the ^{15}O(α, γ)^{19}Ne reaction [2] and is further facilitated at increasing temperatures by ^{4}He(2 ^{4}He,γ)^{12}C(2p,γ)^{14}O(α, p)^{17}F(p,γ)^{18}Ne(α,p)^{21}Na that feeds continuously the αp process [3,4] via the ^{21}Na(p,γ)^{22}Mg(α,p)^{25}Al(p,γ)^{26}Si reaction.

The αp process is a sequence of α- and proton-induced reactions that transport rapidly material, along the neutron-deficient side of the stable nuclei, from the CNO cycle toward heavier masses in the Ca/Ti region as shown in Fig. 1. This causes a rapid release of energy driving the thermonuclear runaway as reflected in the rapid rise time of the XRB light curve. The reaction rates of the (α,p) reaction processes along

[*]Present address: IBA Particle Therapy, Am Mühlenbach 1, DE-45147 Essen, Germany.
[†]Present address: GSI Helmholtzzentrum für Schwerionenforschung GmbH, Planckstraße 1, DE-64291 Darmstadt, Germany.
[‡]Present address: INCAS3, Assen, The Netherlands.
[§]Present address: Center for Nuclear Study, University of Tokyo, Wako, Saitama 351-0198, Japan.
[‖]Present address: Office for Development of Proton Therapy Center, Regional Health Services Division, Department of Health and Welfare Fukui Prefectural Government, Fukui City, Fukui Prefecture 910-0846, Japan.

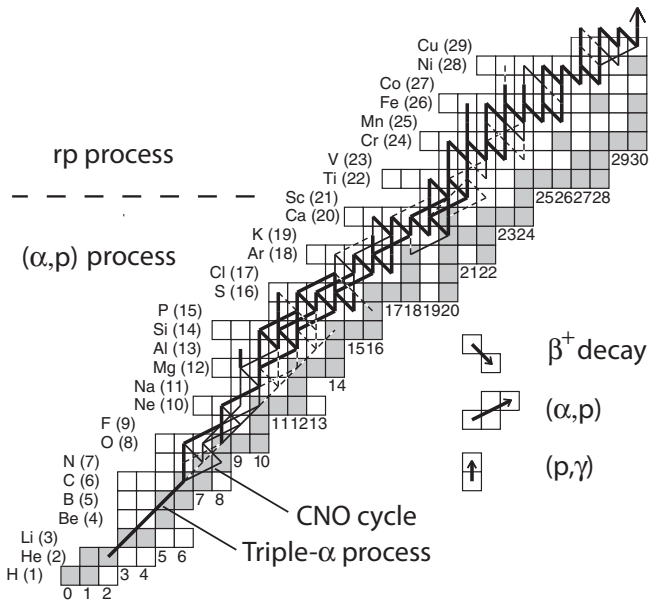

FIG. 1. The time-integrated reaction flow during the thermonuclear runaway at the surface of an accreting neutron star. After breakout from the hot CNO cycle, the flow pattern is characterized by the αp process, which turns into an rp-process pattern starting in the Ca/Ti mass region. Details are given in the text.

the reaction path have a direct effect on the rise time of the light curve and can even influence its overall shape [5].

The rates for the various (α,p) reactions associated with the thermonuclear runaway are based on theoretical predictions using the Hauser-Feshbach model [3,4] since no direct experimental data are available. The applicability of the Hauser-Feshbach approach depends sensitively on the resonance density in the compound nucleus [6], but the resonance density in the sd-shell compound nuclei ^{18}Ne, ^{22}Mg, ^{26}Si, ^{30}S along the αp process path is limited, in particular since only natural parity states can be populated in spin-zero α capture [7]. This suggests that the actual reaction rate may differ substantially from the rates predicted by the statistical model. This was indeed demonstrated in a recent ^{24}Mg$(p,t)^{22}$Mg experiment to study the level structure of ^{22}Mg, the compound nucleus of the ^{18}Ne$(\alpha,p)^{21}$Na reaction [8]. Based on these experimental results, a reaction rate was derived that deviates substantially from the Hauser-Feshbach predictions. The change in this reaction rate translates into a substantial change for the XRB light-curve predictions.

This paper focuses on the ^{22}Mg$(\alpha,p)^{25}$Al reaction using similar experimental and theoretical techniques for deriving the reaction rate. Previous work is primarily based on the assumption of a Hauser-Feshbach rate, but so far, there has been only extremely limited experimental information available about the level structure of the compound nucleus ^{26}Si above the α-emission threshold of 9.164 MeV. Previous experiments were focused on studying the nuclear structure and shell-model interpretations of proton-bound states [9] and proton-unbound but α-bound states [10]. This experiment is the first study seeking to investigate the range of higher excitation energies of α-unbound states to identify possible resonances for the astrophysically relevant ^{22}Mg$(\alpha,p)^{25}$Al reaction.

In Sec. II, we describe the experimental setup and techniques used in this study; this will be followed by the analysis of the experimental results and the approach to determine the level parameters of the observed states such as spin and parity in Sec. III. In Sec. IV, we use this information to derive the reaction rate and to compare it to a number of presently available Hauser-Feshbach predictions using a variety of different models.

II. EXPERIMENTAL TECHNIQUE AND CALIBRATION

In this paper, we report the measurement of ^{26}Si levels above the α-emission threshold. To identify resonance levels for the ^{22}Mg$(\alpha,p)^{25}$Al reaction, we performed a ^{28}Si$(p,t)^{26}$Si experiment at the Ring Cyclotron facility of the Research Center for Nuclear Physics (RCNP) at Osaka University. This measurement used the same technique as our previous study of the ^{24}Mg$(p,t)^{22}$Mg reaction [8]. The details of the experimental technique and the data analysis are discussed extensively in previous works [8,10] and are therefore only summarized briefly here.

A 98.7-MeV proton beam from the Ring Cyclotron was transported via the "fully dispersion-matched" WS beam line [11] to a target chamber. The proton beam impinged on a 0.7-mg/cm^2 thick ^{28}Si self-supporting target [12] consisting of a stack of three thin foils. The outgoing tritons were momentum analyzed by the Grand Raiden (GR) spectrometer [13]. For the identification and subtraction of events from ^{12}C and ^{16}O contaminants, a 1-mg/cm^2 thick ^{12}C target and a 1-mg/cm^2 thick Mylar target were used.

The goal of this experiment was to investigate the nuclear structure of ^{26}Si from the ground state up to 12 MeV excitation energy. Because of the small momentum acceptance of 5% of GR [13], we performed measurements at three different magnetic settings in order to collect overlapping spectra from the ground state to 12 MeV excitation energy. Furthermore, we performed measurements at three different angles: -0.3°, 8°, and 17°. In this paper, we discuss ^{26}Si levels above the α-emission threshold of 9.164 MeV.

The calibration of ^{28}Si$(p,t)^{26}$Si spectra above the α-emission threshold was done by using the well-known low-lying states as described in Ref. [10]. The absolute calibration of the focal-plane position versus B_ρ was performed by using the calibration of ^{24}Mg(p,t)^{22}Mg spectra (see Ref. [8]). Therefore, the calculated ^{26}Si excitation energies are sensitive to the uncertainty of 100 keV of the beam energy. This translates into an error of 1.5 keV in the excitation energies in ^{26}Si. Additional systematic errors originate from uncertainties of the reaction-angle determination and the mass of ^{26}Si (1 keV). These systematic errors are quadratically added to obtain the total systematic error. Also, the x position of the fitted peaks has an uncertainty depending on the number of counts in the peak. These errors are as small as about 1 keV for low-lying levels with a high number of accumulated counts and as large as 25 keV at high-lying states with a smaller number of

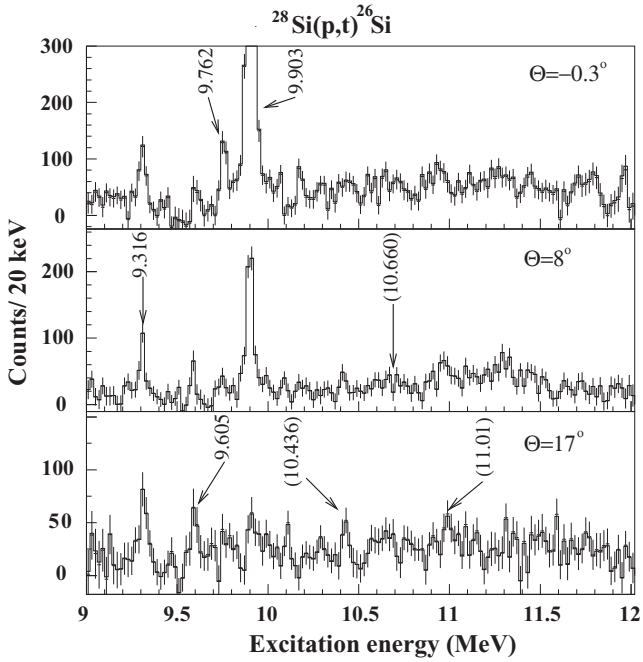

FIG. 2. The ^{28}Si(p,t)^{26}Si spectra above the α-emission threshold measured at -0.3°, 8°, and 17° spectrometer angles. The background from ^{10}C and ^{14}O impurities was subtracted. The energy determined for each peak is marked in the spectrum used to determine it. The determined excitation energies for ^{26}Si are listed in the second column of Table I.

counts. These errors and the total systematic errors are added quadratically to give the total errors shown in Table I.

III. EXPERIMENTAL RESULTS: LEVELS ABOVE THE α-EMISSION THRESHOLD

The ^{26}Si levels above the α-emission threshold are expected to characterize the resonant cross section of the ^{22}Mg(α,p)^{25}Al reaction. In the present experiment, we identified four ^{26}Si levels above the α-emission threshold. The data indicate three more levels for which tentative excitation energies have been determined. These levels are shown in Fig. 2 and are listed in Table I. Possible correspondence to states in the mirror nucleus ^{26}Mg [14] is given in column 3 of Table I, with spin-parity assignments in column 1.

TABLE I. Levels observed above the α-emission threshold at 9.164 MeV in ^{26}Si.

J^π mirror	E_x ^{26}Si (MeV)	E_x ^{26}Mg (MeV)
[4^+]	9.316(5)	9.579(3)
[2^+]	9.605(10)	9.85652(6)
[5^-]	9.762(4)	10.040(2)
[0^+]	9.9034(20)	10.159(3)
	[10.436(10)]	
	[10.66(2)]	
	[11.01(3)]	

For these high excitation energies, the spectrum is characterized by a continuous background, which could result from the excitation of a number of weakly populated natural-parity states of different multipolarities in ^{26}Si. Therefore, an unambiguous identification of states is difficult since a much higher number of levels could be present. For this work, we consider levels to be unambiguously identified if they can be seen at all three angles. The three levels above 10.0 MeV are assigned as tentative since they could only be identified at a consistent excitation energy in two of the three measured spectra. The reason for this conservative approach is the overall low statistics in the data and the obstruction by ^{10}C and ^{14}O impurity lines. We fitted the background in the region between 10 and 12 MeV for all three angles with a constant straight line and obtained a reduced chi-square of around unity. At high level densities where the average level spacing is small compared to the level widths, statistical fluctuations, also known as Ericson fluctuations [15], can occur. The widths of these fluctuations are similar to the widths of the underlying levels. It is, therefore, possible that the peaks observed above 10 MeV excitation energy listed in Table I are fluctuations and not individual levels.

Since the level density in the mirror nucleus ^{26}Mg in this excitation-energy range is very high, it can be assumed that the level density in ^{26}Si is similarly high. Therefore, it is not possible to assign the levels observed in ^{26}Si unambiguously with known levels in ^{26}Mg. From Ref. [10], it can be seen that corresponding levels in the ^{26}Mg mirror nucleus are typically higher by 250 and 350 keV compared to ^{26}Si. This difference was maintained for the mirror assignments discussed here. Because the (p,t) reaction preferably excites natural-parity states, we correlated observed ^{26}Si levels with known natural-parity states in ^{26}Mg. In this way, we obtained the mirror assignments presented in Table I.

IV. ASTROPHYSICAL IMPLICATIONS

^{22}Mg plays a significant role in the reaction flow of the αp process. Because of the fairly long half-life of 3.86 s and the low-Q value of the ^{22}Mg(p,γ)^{23}Al reaction, its rapid depletion in the thermonuclear runaway is hindered and the nucleus represents a waiting point, which can only be bridged by the ^{22}Mg(α, p)^{25}Al reaction. There are no published experimental data for the level structure of the compound nucleus ^{26}Si in the relevant energy region above the α threshold, and this paper presents the first spectrum of states, which allows us to estimate the ^{22}Mg(α, p)^{25}Al reaction rate. The identification of spin and parity for the observed resonance levels relies on the comparison with the level structure of the ^{26}Mg mirror nucleus as discussed in the previous section, given in Table I.

Each of the presently measured resonances has a resonance width that is less than 10% of its resonance energy. This is demonstrated in Fig. 3, which shows the calculated full single-particle widths Γ_p as a function of the c.m. proton energy $E_{\text{c.m.}}$ for the angular momenta $\ell = 0 - 4$. For proton energies $E_{\text{c.m.}} > 2$ MeV, the proton widths Γ_p are of the same order of magnitude as the proton energy for $\ell = 0$ and much

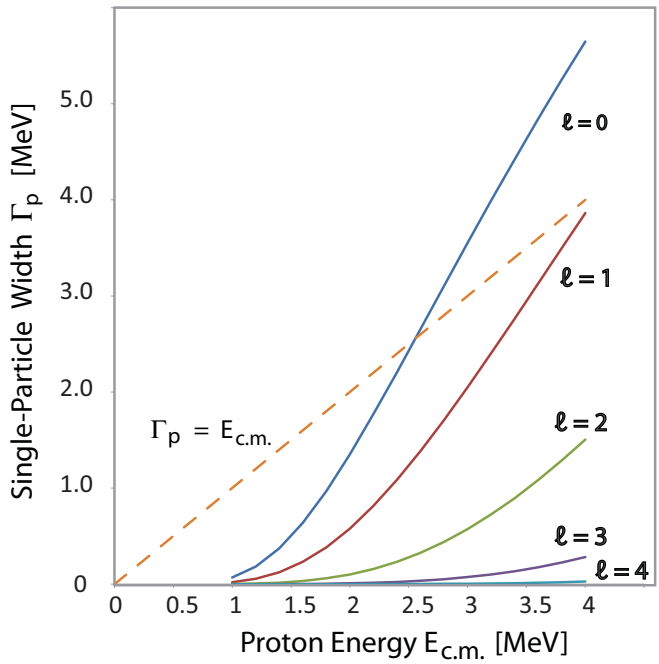

FIG. 3. (Color online) The transmission widths as a function of excitation energy for angular momenta $\ell = 0$, 1, 2, 3, and 4.

smaller for larger ℓ. In this energy range, the levels have a very small proton single-particle configuration and, therefore, their widths are typically two to three orders of magnitude smaller than the full single-particle widths.

Therefore, we used the narrow resonance formalism outlined in Ref. [16]. The total reaction rate can be expressed as the sum of individual resonances

$$N_A\langle\sigma\upsilon\rangle = 1.54\times10^5(\mu T)^{-3/2}\sum_i(\omega\gamma)_i \times \exp(-11.605E_i/T)[\mathrm{cm^3s^{-1}mol^{-1}}] \quad (1)$$

with μ the reduced mass of the target and projectile in units of amu, T the temperature in units of GK, $(\omega\gamma)_i$ the strength in units of eV, and E_i the energy of the ith resonance in units of MeV.

It can be seen from Eq. (1) that the largest uncertainties in the reaction-rate calculations are introduced by uncertainties in the resonance energy because of the exponential dependence. However, with the accuracy of the resonance energies resulting from this experiment, this error is very much reduced and errors in the ^{22}Mg$(\alpha,p)^{25}$Al rate calculations are dominated by the uncertainty of the resonance strengths. Presently, there are no experimental data available for determining the resonance strengths.

The resonance strength is characterized by the spin J of the resonance level and the α and proton partial widths Γ_α and Γ_p of the unbound state in ^{26}Si:

$$\omega\gamma = (2J+1)\frac{\Gamma_\alpha\Gamma_p}{\Gamma}, \quad (2)$$

with Γ being the total width, i.e., the sum of the partial widths $\Gamma = \Gamma_\alpha + \Gamma_p + \Gamma_\gamma$. In the case discussed here, the proton partial width is much larger than the α partial width; low-energy α decay is strongly hindered by the Coulomb barrier. The γ partial width is also considerably smaller than the proton width. Equation (2) simplifies then to

$$\omega\gamma = (2J+1)\cdot\Gamma_\alpha. \quad (3)$$

The α partial width Γ_α is the product of the transmission probability of alpha particles through the Coulomb and centrifugal barrier of the ^{22}Mg nucleus and the α-spectroscopic factor S_α of the resonance level. The transmission probability has been calculated in the framework of a Woods-Saxon potential model for an interaction radius of $R_n = 3.5$ fm. Details of the formalism used for the calculations can be found in Ref. [17].

In order to assign S_α values for the ^{26}Si resonance levels observed in this experiment, we adopted the previously discussed spin-parity assignments of Table I. The S_α spectroscopic factors are based on the corresponding values of the mirror levels in ^{26}Mg in that excitation-energy range. A direct mirror assignment is not possible because of the complexity of the level structure so we adopted typical values obtained in ^{22}Ne(^{6}Li,d)^{26}Mg alpha transfer experiments [18] and the resonance strength analysis of the mirror reaction ^{22}Ne$(\alpha,n)^{25}$Mg after correcting for the transmission probabilities [19]. The results are shown in Table II and have served as the guide for the here adopted choices summarized in Table III.

Based on this analysis of ^{26}Mg states, the S_α values of 0.015 and 0.037 were adopted for the 4^+ and 2^+ levels, respectively, since they are based on averaged experimental values [18] in comparison to higher excited 2^+ states for which a reduced alpha strength is anticipated. No 0^+ level has been observed in ^{26}Mg, therefore, an S_α value of 0.037 for the 2^+ level was adopted for the 0^+ level. For the 5^- level, the S_α value of 0.007 of the 1^- state in ^{26}Mg at 11.153 MeV was adopted since that is the only observed negative-party state in the mirror nucleus ^{26}Mg. The here adopted S_α values and, therefore, also the resulting resonance strengths, are typical values in the $A = 22$ system, but we anticipate that they can fluctuate within an order of magnitude due to the uncertainties in the choice of mirror assignment. This range of fluctuation is also reflected in the

TABLE II. The S_α parameters for the ^{22}Ne$(\alpha,n)^{25}$Mg reaction taken from Ref. [19].

E_x (^{26}Mg) (MeV)	E_{res} (MeV)	J^π	S_α
10.693	0.078	4^+	1.49×10^{-2}
10.945	0.330	$2^+, 3^-$	3.71×10^{-2}
11.112	0.497	2^+	3.51×10^{-3}
11.153	0.538	1^-	7.24×10^{-3}
11.163	0.548	2^+	3.51×10^{-3}
11.171	0.556	2^+	3.54×10^{-3}
11.183	0.568	1^-	3.62×10^{-3}
11.194	0.579	2^+	3.46×10^{-3}
11.274	0.659	2^+	3.53×10^{-3}
11.286	0.671	1^-	3.64×10^{-3}
11.310	0.695	1^-	2.91×10^{-2}
11.326	0.711	1^-	2.91×10^{-2}
11.328	0.713	1^-	1.14×10^{-1}

TABLE III. The adopted S_α and spin values and resonance strengths for the four resonances in the ^{22}Mg$(\alpha,p)^{25}$Al reaction.

E_x (^{26}Si) (MeV)	E_{res} (MeV)	J^π	S_α	J	Mirror[a] $\omega\gamma$ (eV)	J	RND1[b] $\omega\gamma$ (eV)	J	RND2[b] $\omega\gamma$ (eV)
9.316	0.152	[4$^+$]	0.015	4	5.81×10^{-37}	1	6.22×10^{-35}	4	5.81×10^{-37}
9.605	0.441	[2$^+$]	0.037	2	1.20×10^{-14}	1	6.66×10^{-15}	0	1.98×10^{-14}
9.762	0.598	[5$^-$]	0.007	5	3.72×10^{-13}	5	3.72×10^{-13}	2	1.23×10^{-10}
9.903	0.739	[0$^+$]	0.037	0	5.14×10^{-08}	0	5.14×10^{-08}	1	1.79×10^{-08}

[a]Spin and resonance strength for the mirror assignments.
[b]Spin and resonance strength for the randomly generated spins of states.

S_α values displayed in Table II. The level density, however, is sufficiently high that these fluctuations may balance. We adopt these values for calculating the resonance strengths as input parameters for determining the reaction rate. In the following, we compare the rate with statistical model predictions to evaluate the uncertainty range further.

Reaction rates for the ^{22}Mg$(\alpha,p)^{25}$Mg reaction were calculated in the temperature range from 0.1 to 10 GK with the spin assumptions and resonance strengths listed in Table III. The results are listed in Table IV. Based on the adopted level parameters, the rates for the four resonance levels were individually calculated and listed in columns 6–9. The sum of all four resonances is listed in column 10 to investigate the range of uncertainty associated with the assumptions for the level parameters. Additional calculations using random spin-parity assignments were performed. In this random selection, spin values of up to the maximum of $\ell = 5$ were used since no level with a spin value of $\ell \geqslant 5$ was observed. The results (RND1, RND2) of the rate calculations are listed in columns 11 and 12 of Table IV.

For comparison, we also calculated rates using several Hauser-Feshbach predictions. The code SMOKER was used adopting level densities from the backshifted Fermi-gas model [20] for ^{26}Si. We also calculated the rates using the codes Non-SMOKER [21], TALYS [22], and CIGAR [23]. The results of SMOKER, Non-SMOKER, and CIGAR are in excellent agreement, as shown in Table IV. However, the results of TALYS are appreciably different.

The predictions (Sum, RND1, and RND2) based on the observed four resonances states with different spin assumptions are shown in Fig. 4 and are compared with the TALYS and non-SMOKER predictions. The resonance-based calculations differ by up to a factor of 3 compared to each other. This is within the uncertainty range associated with the radial dependence of the penetrability calculation. This indicates that, after the here presented improvements in the determination of resonance states and resonance energies, the largest contribution to the uncertainty in the calculated rates is due to the unknown values for the spin and parity. This uncertainty is also larger than the uncertainty introduced by the S_α values used in deriving the α partial widths.

The contributions of the reaction rates from all four resonances are shown seperately in Fig. 5 together with the predictions for the total rate (Sum). The 0.441-MeV resonance yields the dominant contribution in the temperature range of 0.1–0.2 GK. The 0.739-MeV resonance yields the dominant contribution in the interval of 0.2–10 GK. The 0.152-MeV resonance is negligible for the reaction rate of ^{22}Mg$(\alpha,p)^{25}$Al and does not contribute at any temperature, regardless of the

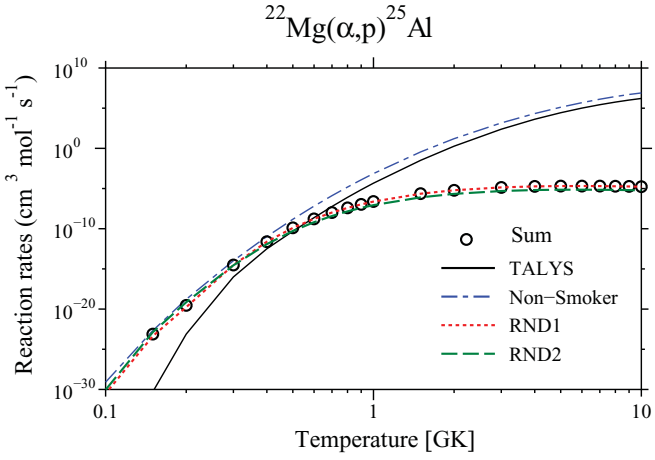

FIG. 4. (Color online) The ^{22}Mg$(\alpha,p)^{25}$Al reaction rate as a function of the temperature for the Hauser-Feshbach predictions TALYS and non-SMOKER and the resonance-based calculations for the assumed (Sum) and random (RND1 and RND2) spin distribution. Note the present resonance-based reaction rate represents a lower limit (see text for details).

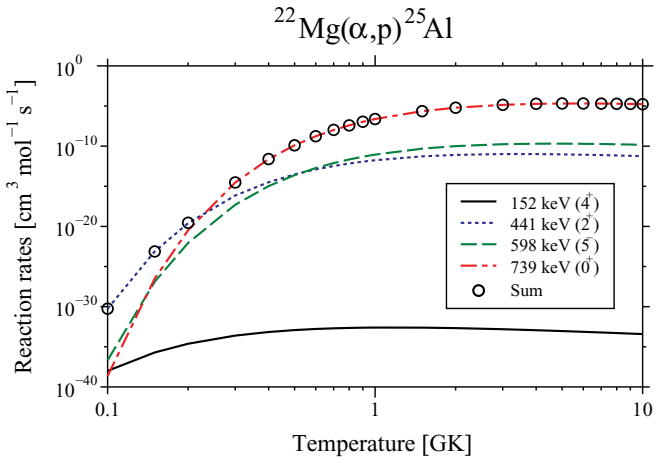

FIG. 5. (Color online) The total ^{22}Mg$(\alpha,p)^{25}$Al reaction rate as a function of the temperature is displayed together with the separate contributions from all four resolved resonances.

TABLE IV. Calculated rates $N_A\langle\sigma\upsilon\rangle$ in units of $cm^3mole^{-1}s^{-1}$ of the $^{22}Mg(\alpha, p)^{25}Al$ reaction as a function of temperature T in units of GK for several statistical models (TALYS, Non-SMOKER, SMOKER, and CIGAR) and the four lowest lying resonances, their sum, and two random spin distributions RND1 and RND2.

T	TALYS	Non-SMOKER	SMOKER	CIGAR	152 keV	441 keV	598 keV	739 keV	Sum	RND1	RND2
0.1	0.00×10^{00}	8.07×10^{-30}	8.25×10^{-30}	8.35×10^{-30}	1.01×10^{-38}	5.57×10^{-31}	2.11×10^{-37}	2.28×10^{-39}	5.57×10^{-31}	3.09×10^{-31}	9.20×10^{-31}
0.15	5.12×10^{-31}	2.12×10^{-23}	2.05×10^{-23}	2.08×10^{-23}	1.96×10^{-36}	7.78×10^{-24}	1.28×10^{-27}	3.23×10^{-27}	7.78×10^{-24}	4.32×10^{-24}	1.33×10^{-23}
0.2	7.80×10^{-24}	1.66×10^{-19}	1.51×10^{-19}	1.55×10^{-19}	2.40×10^{-35}	2.56×10^{-20}	8.76×10^{-23}	3.39×10^{-21}	2.90×10^{-20}	1.77×10^{-20}	7.23×10^{-20}
0.3	9.95×10^{-17}	1.05×10^{-14}	9.19×10^{-15}	1.04×10^{-14}	2.48×10^{-34}	2.56×10^{-20}	5.03×10^{-18}	2.97×10^{-15}	3.05×10^{-15}	3.02×10^{-15}	2.82×10^{-15}
0.4	3.21×10^{-13}	1.08×10^{-11}	1.04×10^{-11}	1.12×10^{-11}	6.99×10^{-34}	3.26×10^{-15}	1.06×10^{-15}	2.45×10^{-12}	2.46×10^{-12}	2.46×10^{-12}	1.21×10^{-12}
0.5	4.87×10^{-11}	1.50×10^{-09}	1.52×10^{-09}	1.57×10^{-09}	1.21×10^{-33}	3.01×10^{-14}	2.44×10^{-14}	1.28×10^{-10}	1.28×10^{-10}	1.28×10^{-10}	5.26×10^{-11}
0.6	2.38×10^{-09}	6.48×10^{-08}	6.57×10^{-08}	6.73×10^{-08}	1.66×10^{-33}	1.26×10^{-13}	1.88×10^{-13}	1.70×10^{-09}	1.70×10^{-09}	1.70×10^{-09}	6.53×10^{-10}
0.7	5.88×10^{-08}	1.30×10^{-06}	1.30×10^{-06}	1.33×10^{-06}	2.00×10^{-33}	3.39×10^{-13}	7.77×10^{-13}	1.04×10^{-08}	1.04×10^{-08}	1.04×10^{-08}	3.87×10^{-09}
0.8	8.09×10^{-07}	1.54×10^{-05}	1.52×10^{-05}	1.55×10^{-05}	2.24×10^{-33}	6.91×10^{-13}	2.20×10^{-12}	3.93×10^{-08}	3.93×10^{-08}	3.93×10^{-08}	1.44×10^{-08}
0.9	7.21×10^{-06}	1.23×10^{-04}	1.20×10^{-04}	1.22×10^{-04}	2.40×10^{-33}	1.18×10^{-12}	4.83×10^{-12}	1.08×10^{-07}	1.08×10^{-07}	1.08×10^{-07}	3.93×10^{-08}
1.0	4.70×10^{-05}	7.35×10^{-04}	7.02×10^{-04}	7.16×10^{-04}	2.49×10^{-33}	1.78×10^{-12}	8.91×10^{-12}	2.40×10^{-07}	2.40×10^{-07}	2.40×10^{-07}	8.64×10^{-08}
1.5	3.29×10^{-02}	3.64×10^{-01}	3.38×10^{-01}	3.44×10^{-01}	2.44×10^{-33}	5.33×10^{-12}	4.90×10^{-11}	2.28×10^{-06}	2.28×10^{-06}	2.28×10^{-06}	8.09×10^{-07}
2.0	$1.88\times10^{+00}$	$1.61\times10^{+01}$	$1.51\times10^{+01}$	$1.54\times10^{+01}$	2.13×10^{-33}	8.12×10^{-12}	1.01×10^{-10}	6.17×10^{-06}	6.17×10^{-06}	6.17×10^{-06}	2.18×10^{-06}
3.0	$2.44\times10^{+02}$	$1.48\times10^{+03}$	$1.47\times10^{+03}$	$1.50\times10^{+03}$	1.56×10^{-33}	1.04×10^{-11}	1.75×10^{-10}	1.40×10^{-05}	1.40×10^{-05}	1.40×10^{-05}	4.94×10^{-06}
4.0	$4.22\times10^{+03}$	$2.16\times10^{+04}$	$2.20\times10^{+04}$	$2.23\times10^{+04}$	1.17×10^{-33}	1.03×10^{-11}	2.03×10^{-10}	1.86×10^{-05}	1.86×10^{-05}	1.86×10^{-05}	6.55×10^{-06}
5.0	$2.74\times10^{+04}$	$1.32\times10^{+05}$	$1.33\times10^{+05}$	$1.35\times10^{+05}$	9.15×10^{-34}	9.54×10^{-12}	2.05×10^{-10}	2.05×10^{-05}	2.05×10^{-05}	2.05×10^{-05}	7.19×10^{-06}
6.0	$1.03\times10^{+05}$	$4.90\times10^{+05}$	$4.80\times10^{+05}$	$4.86\times10^{+05}$	7.38×10^{-34}	8.61×10^{-12}	1.97×10^{-10}	2.07×10^{-05}	2.07×10^{-05}	2.07×10^{-05}	7.28×10^{-06}
7.0	$2.72\times10^{+05}$	$1.32\times10^{+06}$	$1.26\times10^{+06}$	$1.28\times10^{+06}$	6.11×10^{-34}	7.71×10^{-12}	1.84×10^{-10}	2.02×10^{-05}	2.02×10^{-05}	2.02×10^{-05}	7.08×10^{-06}
8.0	$5.73\times10^{+05}$	$2.82\times10^{+06}$	$2.69\times10^{+06}$	$2.72\times10^{+06}$	5.16×10^{-34}	6.92×10^{-12}	1.71×10^{-10}	1.92×10^{-05}	1.92×10^{-05}	1.92×10^{-05}	6.75×10^{-06}
9.0	$1.03\times10^{+06}$	$5.08\times10^{+06}$	$4.94\times10^{+06}$	$5.00\times10^{+06}$	4.43×10^{-34}	6.22×10^{-12}	1.58×10^{-10}	1.82×10^{-05}	1.82×10^{-05}	1.82×10^{-05}	6.37×10^{-06}
10.0	$1.63\times10^{+06}$	$7.93\times10^{+06}$	$8.16\times10^{+06}$	$8.24\times10^{+06}$	3.86×10^{-34}	5.63×10^{-12}	1.45×10^{-10}	1.71×10^{-05}	1.71×10^{-05}	1.71×10^{-05}	5.99×10^{-06}

choice for the spin value. With the adopted spin value of 0^+ for the 0.739-MeV resonance, it completely dominates the reaction rate for temperatures above 0.2 GK. However, if the 0.598-MeV resonance has spin 0^+, this resonance will become stronger at temperatures above 0.2 GK.

Table IV and Fig. 4 also indicate that the present predictions for the reaction rate are in agreement with the Hauser-Feshbach statistical calculations up to 0.4 GK stellar temperature. The large discrepancy between these models at temperatures higher than 0.4 GK may be explained by the lack of resonance data above 10-MeV excitation energy in ^{26}Si. Possible additional resonances above 0.75 MeV are indicated in Table III and will enhance the ^{22}Mg$(\alpha,p)^{25}$Al reaction rates at temperatures above 0.4 GK. Therefore, the Hauser-Feshbach prediction can be considered as an upper limit for the reaction rate above 0.4 GK and our experimental reaction rate as a lower limit.

V. CONCLUSIONS

We have presented experimental results of resonance states above the α threshold to calculate the reaction rates of the ^{22}Mg$(\alpha,p)^{25}$Al reaction using the narrow resonance formalism. The remaining uncertainty in the reaction rates is dominated by the unknown values of the spins and parities of these resonance states. To further improve the precision of the reaction rates, direct measurements in inverse kinematics are planned using the radioactive beam and a new recoil separator at the ReA3 facility at NSCL.

[1] S. E. Woosley, A. Heger, A. Cumming, R. D. Hoffman, J. Pruet, T. Rauscher, J. L. Fisker, H. Schatz, B. A. Brown, and M. Wiescher, Astrophys. J., Suppl. Ser. **151**, 75 (2004).

[2] J. L. Fisker, W. Tan, J. Görres, M. Wiescher, and R. L. Cooper, Astrophys. J. **665**, 637 (2007).

[3] S. E. Woosley and R. K. Wallace, Astrophys. J., Suppl. Ser. **45**, 389 (1981).

[4] L. van Wormer, J. Görres, C. Iliadis, M. Wiescher, and F.-K. Thielemann, Astrophys. J. **432**, 326 (1994).

[5] J. L. Fisker, F.-K. Thielemann, and M. Wiescher, Astrophys. J. Lett. **608**, L61 (2004).

[6] T. Rauscher, F.-K. Thielemann, and K.-L. Kratz, Phys. Rev. C **56**, 1613 (1997).

[7] T. Rauscher, F.-K. Thielemann, J. Görres, and M. Wiescher, Nucl. Phys. A **675**, 695 (2000).

[8] A. Matic, A. M. van den Berg, M. N. Harakeh, H. J. Wörtche, G. P. A. Berg, M. Couder, J. L. Fisker, J. Görres, P. Leblanc, S. O'Brien *et al.*, Phys. Rev. C **80**, 055804 (2009).

[9] P. M. Endt, Nucl. Phys. A **521**, 1 (1990), and references therein.

[10] A. Matic, A. M. van den Berg, M. N. Harakeh, H. J. Wörtche, G. P. A. Berg, M. Couder, J. Görres, P. Leblanc, S. O'Brien, M. Wiescher *et al.*, Phys. Rev. C **82**, 025807 (2010), and references therein.

[11] T. Wakasa, K. Hatanaka, Y. Fujita, G. P. A. Berg, H. Fujimura, H. Fujita, M. Itoh, J. Kamiya, T. Kawabata, K. Nagayama *et al.*, Nucl. Instrum. Methods Phys. Res., Sect. A **482**, 79 (2002).

[12] J. P. Greene and G. P. A. Berg, Nucl. Instrum. Methods Phys. Res., Sec. B **241**, 1006 (2005).

[13] M. Fujiwara, H. Akimune, I. Daito, H. Fujimura, Y. Fujita, K. Hatanaka, H. Ikegami, I. Katayama, K. Nagayama, N. Matsuoka *et al.*, Nucl. Instrum. Methods Phys. Res., Sect. A **422**, 484 (1999).

[14] P. M. Endt, Nucl. Phys. A **633**, 1 (1998).

[15] T. Ericson, Ann. Phys. (NY) **23**, 390 (1963).

[16] C. E. Rolfs and W. S. Rodney, *Cauldrons in the Cosmos* (University of Chicago Press, Chicago, 1988).

[17] C. Iliadis, Nucl. Phys. A **618**, 166 (1997).

[18] U. Giesen, C. P. Browne, J. Görres, S. Graff, C. Iliadis, H.-P. Trautvetter, M. Wiescher, W. Harms, K. L. Kratz, B. Pfeiffer, R. E. Azuma, M. Buckby, and J. D King, Nucl. Phys. A **561**, 93 (1995).

[19] A. I. Karakas, M. A. Lugaro, M. Wiescher, J. Görres, and C. Ugalde, Astrophys. J. **643**, 471 (2006).

[20] A. Gilbert and A. G. W. Cameron, Can. J. Phys. **43**, 1446 (1965).

[21] Non-SMOKER [http://nucastro.org/nonsmoker.html].

[22] TALYS [http://www-astro.ulb.ac.be/Nucdata/Talys/pcapAL].

[23] CIGAR, R. Crowter, MS Phys. Thesis, University of Surrey, UK, 2007.